One-Dimensional Phase Transformation Model and Its Application to Damping Enhancement Analysis

Tadashige Ikeda

Abstract A simple yet reasonably accurate constitutive model of shape memory alloys (SMAs) has been developed. It can treat more than three phases or/and variants and duplicate their rate-dependent deformation behavior quantitatively. This model was applied to damping enhancement analysis. Damping oscillations of cantilever beams with various SMA foils bonded on their both surfaces were simulated numerically. It was seen that bonding SMA foils is effective for the damping enhancement in some cases. Furthermore, it was found that adequate mechanical or/and thermal treatment for SMA foils improves the damping performance.

Keywords Shape memory alloys · Constitutive equations · Damping enhancement · Numerical simulation

1 Introduction

Shape memory alloys (SMAs), for instance TiNi SMA, have elastic modulus of 20–100 GPa and strength of 1000–2000 MPa. In addition they deform elastically or thermally with 6–8% strain, generate stress of 500–900 MPa, and change their electrical resistance depending on temperature (Otsuka and Wayman 1998). Due to these properties, they can be used as structural elements with functions of actuators, sensors, etc. Accordingly, they are applied in wide range of field such as aerospace, medical, and livingware, since the number of parts and complexity of a system can be reduced by using them (Otsuka and Wayman 1998; Yamauchi et al. 2011). However, deformation behavior based on phase transformation is complicated having hysteresis whose shape is affected by temperature and loading frequency.

T. Ikeda (✉)
Department of Aerospace Engineering, Furo-cho, Chikusa-ku, Nagoya 464-8603, Japan
e-mail: ikeda@nuae.nagoya-u.ac.jp

Q. Sun et al. (eds.), *Advances in Shape Memory Materials*,
Advanced Structured Materials 73, DOI 10.1007/978-3-319-53306-3_2

To understand the mechanism of such a complicated behavior and design products including SMAs optimally, fundamental experimental data and mathematical models are necessary, and many experimental and mathematical studies have been performed (Otsuka and Ren 2005; Tobushi et al. 2013; Machado and Lagoudas 2008; Barbarino et al. 2014).

Regarding the constitutive models, for example, Falk (1983) proposed a model which obtains stress versus strain relationship by differentiating a free energy function assumed to be a polynomial of strain and temperature. Müller (1989) and Seelecke (1996) expressed the free energy function as a sum of the free energy functions multiplied by a fraction of each phase and introduced interfacial energy between domains additionally. Bertram (1982), Tanaka (1986), and others (Liang and Rogers 1990; Brinson 1993; Sun and Hwang 1993; Boyd and Lagoudas 1996; Raniecki et al. 1992; Ivshin and Pence 1994; Leclercq and Lexcellent 1996; Kamita and Matsuzaki 1998; Matsuzaki et al. 2001) have presented models which express transformation process between martensite phase and austenite phase or/and among martensite variants by considering internal variables and the energy dissipation like models in plastic deformation. Historical summary of these types of models were presented by Machado and Lagoudas (2008). Patoor et al. (1995), and others (Gall and Sehitoglu 1999; Nae et al. 2003) presented models which obtain macroscopic behavior by averaging variables in microscopic behavior of individual grains where shape memory alloy was assumed to consist of a number of grains. Graesser and Cozzarelli (1991) and Ortín (1992) expressed the hysteresis of the deformation behavior mathematically without respect to detail physical phenomena.

The present author and his co-workers (Nae et al. 2003; Ikeda et al. 2004; Ikeda 2005, 2008) have proposed several types of constitutive models. To understand the behavior of partial transformation theoretically, they proposed a grain-based micromechanical constitutive model (Nae et al. 2003). By mathematically increasing number of the grains to infinity in the micromechanical model, another type of lumped parameter models referred to as the one-dimensional phase transformation model was obtained (Ikeda et al. 2004). Moreover, this model was extended so as to be able to describe tension-compression asymmetric behavior (Ikeda 2005, 2008) and tension-torsion behavior (Ikeda 2006).

Among the smart materials composing the smart structures, SMA is one of the most promising materials because it has functions as an actuator and a sensor in addition to enough strength and stiffness as a structural element, as described. Moreover it is expected to be used as a damping material because of existence of a large hysteresis loop in stress-strain relationship. Thomson et al. (1995) and others (Gandhi and Chapuis 2001; Boller et al. 2001) showed the damping of a beam increased significantly with SMA wires. In their studies SMA wires were connected to the beam with an angle such that the wires vibrate with a large strain amplitude. In real situation, however, SMA would be often bonded on or embedded into a structural element, where the strain amplitude is much smaller than their studies. Hence we examined the effect of SMA foils bonded on the surface of structural elements on damping enhancement by experiment and calculation (Ikeda et al. 2004).

In this paper, we introduce our constitutive model of SMA referred to as one-dimensional phase transformation model (Ikeda et al. 2004; Ikeda 2005, 2008) and application of the model to the damping enhancement analysis of SMA foils bonded on a base structure (Ikeda et al. 2004).

2 One-Dimensional Phase Transformation Model

2.1 Constitutive Model

The concept of the one-dimensional phase transformation model is illustrated in Fig. 1. Here we consider a SMA bar specimen. The specimen is assumed to consist of three phases; an austenitic phase (A), a tensile stress induced martensitic phase (T), and a compressive stress induced martensitic phase (C). RTE is defined as the energy required for the phase transformation, which is caused by the interaction between grains or phases. It is assumed that infinitesimal grains in the bar specimen are sorted in order of RTE, so that RTE takes the minimum value at the bottom and the maximum value at the top. The order of these grains is assumed to be unchanged irrespective of the phases before and after the transformation. Accordingly, any phase transformation proceeds from the lower part to the upper part of the bar specimen one-dimensionally. Hence, this model is referred to as the one-dimensional phase transformation model. Since this model is a lumped parameter model, distribution of the grains does not affect its characteristics. A sum of ranges for each phase corresponds to the volume fraction of the phase, when the distance from the bottom is normalized with the length of the bar specimen. Hence, the ordinate is named the volume fraction coordinate (VFC).

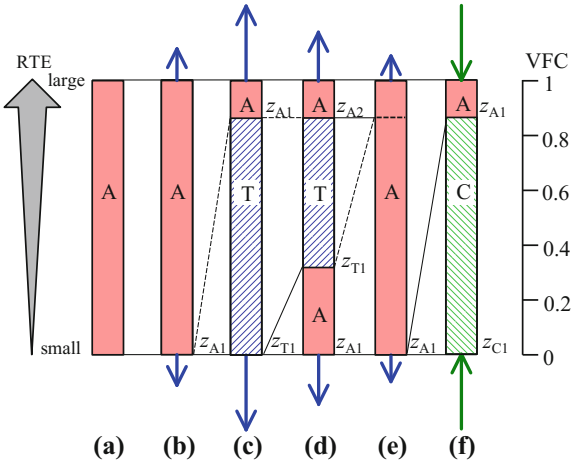

Fig. 1 Concept of one-dimensional phase transformation rule. *A*, *T*, and *C* represent the austenitic phase. Tensile stress induced martensitic phase, and compressive stress induced martensitic phase. *RTE* is the required transformation energy and *VFC* is the volume fraction coordinate. See the text for details

First, a whole specimen is assumed to be in phase A (Fig. 1a). When a tensile force is applied to the bar (Fig. 1b) and the stress value increases beyond a certain critical value, the transformation from phase A to phase T takes place from the bottom, at which RTE takes the minimum value (Fig. 1c). Then, when the tensile force is removed and the stress value decreases below another certain critical value, the reverse-transformation from phase T to phase A takes place from the bottom (Fig. 1d, e). A compressive force is applied and the magnitude of the negative stress value increases beyond another certain critical value, the transformation from phase A to phase C takes place from the bottom (Fig. 1f).

According to this assumption, the transformation criterion from phase α to phase β is formulated as

$$\frac{1}{2}\sigma^2\left(\frac{1}{E_\beta}-\frac{1}{E_\alpha}\right)+\sigma(\varepsilon_\beta-\varepsilon_\alpha)+(s_\beta-s_\alpha)(T-T_{\alpha\leftrightarrow\beta})=\Psi_{\alpha\to\beta}(z_{\alpha 1}), \tag{1}$$

The left hand side is the thermomechanical driving energy for transformation from phase α to phase β and the right hand side $\Psi_{\alpha\to\beta}$ is RTE for the transformation from phase α to phase β. σ, E_α, ε_α, s_α, T, and $T_{\alpha\leftrightarrow\beta}$ denote the stress, the Young's modulus for phase α, the intrinsic strain due to the crystal structure of phase α, the entropy for phase α, the material temperature, and the ideal transformation temperature between phase α and phase β without dissipation due to the internal friction. $z_{\alpha 1}$ in the right hand side denotes VFC with the minimum energy value of phase α as shown in Fig. 1.

It was found from measured data that RTEs can be approximated by a sum of two exponential functions in terms of $z_{\alpha\to\beta}$ and $1–z_{\alpha\to\beta}$ as

$$\Psi_{\alpha\to\beta}=\Psi_{\mathrm{c1},\alpha\to\beta}+\Psi_{\mathrm{c2},\alpha\to\beta}\left[1-a_{1,\alpha\to\beta}{}^{-z_{\alpha\to\beta}}+b_{\alpha\to\beta}a_{2,\alpha\to\beta}{}^{-(1-z_{\alpha\to\beta})}\right], \tag{2}$$

where $\Psi\mathrm{c1}_{,\alpha\to\beta}$, $\Psi\mathrm{c2}_{,\alpha\to\beta}$, $a_{1,\alpha\to\beta}$, $b_{\alpha\to\beta}$, and $a_{2,\alpha\to\beta}$ are the material constants.

The strain is assumed to be a sum of the elastic strain, the intrinsic strain, and the thermal strain, and written as

$$\varepsilon=\sigma\sum_\alpha\frac{z_\alpha}{E_\alpha}+\sum_\alpha z_\alpha\varepsilon_\alpha+\alpha_{\mathrm{T}}(T-T_{\mathrm{r}}), \tag{3}$$

where α_{T}, T_{r}, and z_α are the coefficient of thermal expansion, the reference temperature, and the volume fraction of phase α.

The energy balance equation is given by

$$C\dot{T}+\sum_{\alpha\to\beta}(s_\beta-s_\alpha)T\dot{z}_{\alpha\to\beta}+\alpha_{\mathrm{T}}T\dot{\sigma}=-h\frac{4}{d}(T-T_{\mathrm{s}})+\sum_{\alpha\to\beta}\Psi_{\alpha\to\beta}\dot{z}_{\alpha\to\beta}, \tag{4}$$

where C, h, d, and T_{S} are the specific heat capacity at constant stress, the convection heat transfer coefficient, the diameter of a bar specimen, and the surrounding

temperature, respectively. The left hand side consists of the sensible heat, the latent heat, and thermoelastic effect, and the right hand side consists of the heat transfer to the surroundings and the heat generated due to the dissipation. The energy balance equation indicates that the reversible heat flow equals a sum of the actual heat flow and the lost work.

2.2 Evaluation of Validity of the Model

The set of Eqs. (1)–(4) can be solved by giving an initial state and an applied stress or strain. To show the ability of the proposed model, numerical simulation was performed. In particular, the effect of loading frequencies was examined. The constants of the SMA wire and its surroundings used in the numerical simulation are listed in Table 1 (Ikeda 2005). It is assumed $T_r = T_S$.

Figure 2a, b show predicted stress-strain hysteresis loops for tension-compression cycles between 8% strain and −4% strain and between 4% strain and –2% strain at a strain rate of 1.0×10^{-4} s^{-1} and at a surrounding temperature of 295 K and 375 K, respectively. The hysteresis loops have asymmetric shapes between tension and compression. Moreover, the first loop is different from the other loops. Magnitudes of the transformation stresses at 375 K are higher than those at 295 K, because the driving energy decreases as temperature increases as can be seen from Eq. (1).

Next the effect of strain rate was examined. Stress-strain relationship for the first fifty 8%/–4% strain cycles at a strain rate of 1.0×10^{-1} s^{-1} and at a surrounding

Table 1 Constants of the wire and surroundings (Ikeda 2005)

E_A GPa	E_T GPa	E_C GPa	ε_A	ε_T	ε_C
74	30	150	0	0.045	–0.026
s_T–s_A MJ/(m^{3}K)	s_C–s_A MJ/(m^{3}K)	s_T–s_C MJ/(m^{3}K)	$T_{A\leftrightarrow T}$ K	$T_{A\leftrightarrow C}$ K	
–0.246	–0.246	0	295	295	
C MJ/(m^{3}K)	α_T K^{-1}	d mm	h W/(m^{2}K)		
3.0	1.0×10^{-5}	3.0	150		
$\alpha \rightarrow \beta$	$\Psi_{c1,\alpha\rightarrow\beta}$ MJ/(m^3)	$\Psi_{c2,\alpha\rightarrow\beta}$ MJ/(m^3)	$a_{1,\alpha\rightarrow\beta}$	$b_{\alpha\rightarrow\beta}$	$a_{2,\alpha\rightarrow\beta}$
A → T	6.5	5.5	10^8	1	10^3
A → C	5.0	3.3	10^2	10	3×10^4
C → T	6.5	5.5	10^8	1	10^3
C → A	5.0	3.3	10^2	10	3×10^4
T → A	0	8.3	10^4	1	10^4
C → A	0	12	10^4	1	10^4

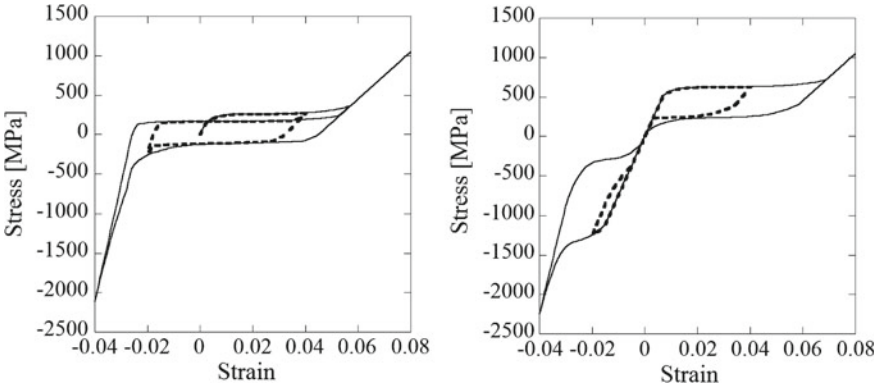

(a) 295K **(b)** 375K

Fig. 2 Stress-strain relationship at a strain rate of 1.0×10^{-4} and at a surrounding temperature of **a** 295 K and **b** 375 K (Ikeda 2005)

temperature of 295 K is shown in Fig. 3a. Thick dashed line and thick solid line represent those for the first cycle and for the fiftieth cycle, respectively. The temperature during the strain cycles is shown in Fig. 3b. The temperature increases by approximately 80 K due to the balance of the dissipated energy and the heat exchange described in the right hand side of Eq. (4). Because of this, the stress-strain relationship for the first cycle is similar to the one in Fig. 2a and the stress-strain relationship for the fiftieth cycle is similar to the one in Fig. 2b. The temperature variation in each cycle is caused by the latent heat and the thermoelastic effect which are related to the second term and the third term of the left hand side of Eq. (4).

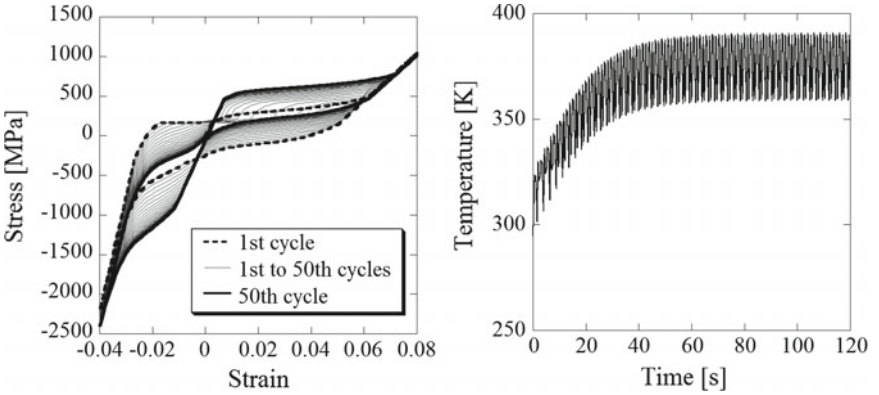

(a) First 50 cycles of stress-strain relationship **(b)** Variation of the material temperature

Fig. 3 Deformation behavior at a strain rate of 1.0×10^{-1} and at a surrounding temperature of 295 K (Ikeda 2005)

3 Damping Enhancement Analysis (Ikeda et al. 2004)

3.1 Governing Equations of a Beam with a Tip Mass and SMA Foils Bonded

Next dynamic behavior of a beam with a tip mass and SMA foils bonded as shown in Fig. 4 is formulated using Bernoulli-Euler beam theory.

Equation of motion of a uniform Bernoulli-Euler beam is

$$\mu \frac{\partial^2 w}{\partial t^2} + E^* I \frac{\partial^4 w}{\partial x^4} = f(x,t), \tag{5}$$

where x, t, μ, $w(x, t)$, and $f(x, t)$ denote the longitudinal coordinate, the time, the mass per unit length, the displacement, and the distributed external force. E^*I is the complex bending stiffness of the beam and given by

$$E^* I = E^*_{\mathrm{Al}} \frac{BH^3_{\mathrm{Al}}}{12} + 2E^*_{\mathrm{Ep}} \frac{BH^3_{\mathrm{Ep}}}{12} + \frac{B}{2} E^*_{\mathrm{Ep}} H_{\mathrm{Ep}} (H_{\mathrm{Al}} + H_{\mathrm{Ep}})^2, \tag{6}$$

where E^*, B, H, and subscripts Al and Ep are the complex Young's modulus, the breadth, the thickness, and the quantities of the aluminum beam and the epoxy adhesive.

Assuming that the displacement is separable in space and time and that the first mode vibration is dominant, that is,

$$w(x,t) = q(t) W(x), \tag{7}$$

one can obtain the following ordinary differential equation,

$$\frac{d^2 q}{dt^2} + \eta \frac{\Omega^2}{\omega} \frac{dq}{dt} + \Omega^2 q = Q. \tag{8}$$

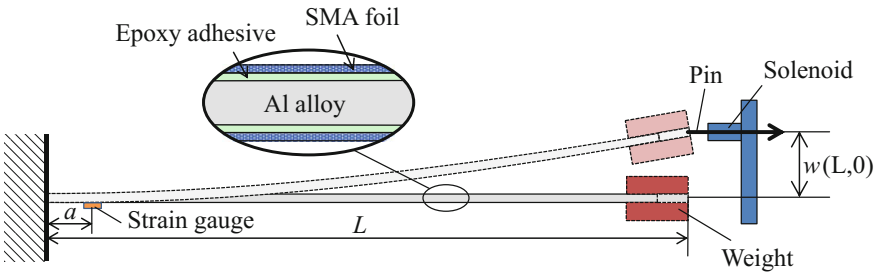

Fig. 4 Schematic of the experimental setup of a sandwiched cantilever beam

q, W, ω, η, and Ω are the generalized coordinate, the eigenfunction, the angular frequency, the damping factor, and the natural angular frequency. Q is the generalized force associated with q, and defined as

$$Q(t) = \int_0^L f(x,t)W(x)dx, \tag{9}$$

where L is the length of the beam. W is normalized as

$$\int_0^L \mu W^2(x)dx = 1. \tag{10}$$

Effect of the tip mass is considered as the external force given by

$$\begin{aligned} Q_{mass} &= \int_0^L -M\frac{\partial^2 w(t,L)}{\partial t^2}\delta(x-L)W(x)dx \\ &= -MW^2(L)\frac{d^2q}{dt^2} \end{aligned} \tag{11}$$

where M and δ denote the mass of the tip mass and the Dirac delta function.

The force from the SMA foil is assumed transmitted as if the concentrated forces act at the edges of the beam. Here we consider only a bending moment and ignore an axial force. The bending moment can be transformed into the equivalent coupling forces f_{SMA} with a distance of 2Δ as shown in Fig. 5 and given by the following equation.

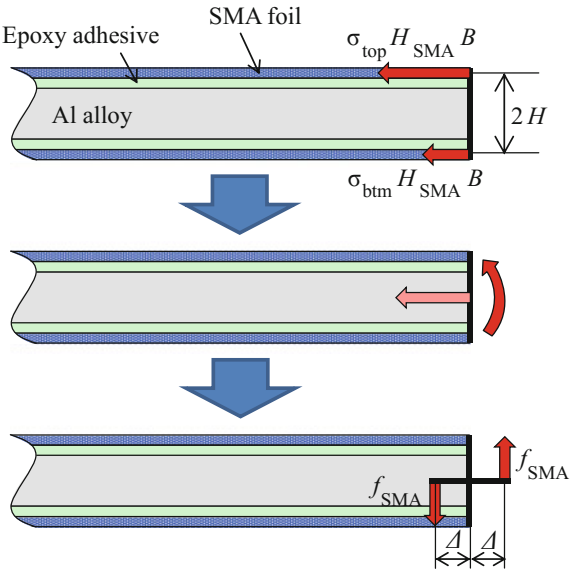

Fig. 5 Coupling forces equivalent to a bending moment due to SMA foils

$$\lim_{\Delta \to 0} f_{\mathrm{SMA}}(2\Delta) = (\sigma_{\mathrm{top}} - \sigma_{\mathrm{btm}}) H H_{\mathrm{SMA}} B, \tag{12}$$

where

$$H = \frac{1}{2} H_{\mathrm{Al}} + H_{\mathrm{Ep}} + \frac{1}{2} H_{\mathrm{SMA}} \tag{13}$$

The subscripts top, btm, and SMA represent the quantities of the top foil, the bottom foil, and SMA foil. Accordingly, the generalized force generated by the SMA foils is obtained as

$$\begin{aligned} Q_{\mathrm{SMA}} &= \lim_{\Delta \to 0} \int_0^{L+\Delta} f_{\mathrm{SMA}} [\delta(x - L - \Delta) - \delta(x - L + \Delta)] W(x) dx \\ &= (\sigma_{\mathrm{top}} - \sigma_{\mathrm{btm}}) H H_{\mathrm{SMA}} B \frac{dW(L)}{dx}. \end{aligned} \tag{14}$$

By integrating the local strain over the beam and by considering the boundary condition, the averaged strain of the top SMA foil is obtained as

$$\varepsilon_{\mathrm{top}} = \varepsilon_{\mathrm{pre}} - \frac{1}{L} \int_0^L \frac{d^2 W}{dx^2} q H dx = \varepsilon_{\mathrm{pre}} - \frac{1}{L} \left[\frac{dW(L)}{dx} \right] q H, \tag{15}$$

where $\varepsilon_{\mathrm{pre}}$ is the prestrain when the foil is bonded. The bottom strain is obtained in a similar way as

$$\varepsilon_{\mathrm{btm}} = \varepsilon_{\mathrm{pre}} + \frac{1}{L} \left[\frac{dW(L)}{dx} \right] q H. \tag{16}$$

3.2 *Experiment of Damping Vibration of Beams with SMA Foil Bonded*

Figure 4 shows a schematic figure of the cantilevered beam used in the damping enhancement measurement. Five types of specimens were made. Those were a just aluminum beam (Al), aluminum beams with bonded SMA foils in R phase at room temperature (Al + R), with bonded SMA foils in austenitic phase (Al + A), with bonded prestrained SMA foils (Al + PA), and with bonded stainless steel foils (Al + S). The prestrain was applied to the austenitic SMA foils expecting SMA to vibrate around the center of the major stress-strain hysteresis loop. The stainless steel foil was used to compare SMA foil with another metal foil. To avoid the effect of aerodynamic damping, the experiment was carried out in a vacuumed camber. In the experiment a beam was first bent by quasistatically, its free end was put on the tip of a pin, and then the beam was released to start a vibration by pulling the pin.

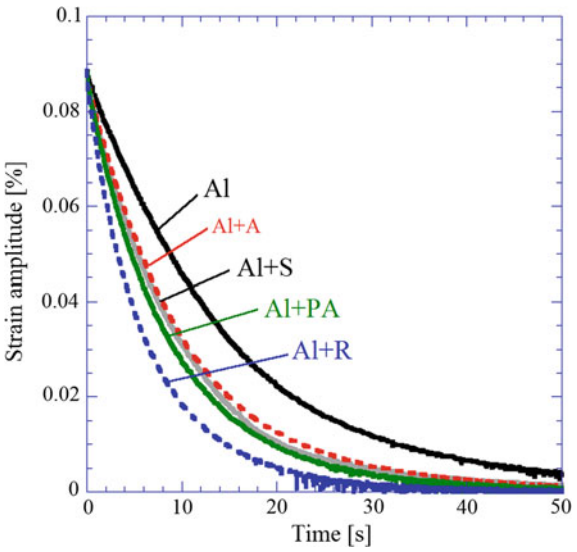

Fig. 6 Measured envelope of damping vibration wave (Ikeda et al. 2004)

The vibration was measured by a strain gauge attached at 30 mm from the clamp on the beam.

Figure 6 shows the envelopes of the positive side of the measured damping vibration of the beams. The damping of Al + R is approximately 200% superior when compared to Al and is approximately 100% superior when compared to Al + S. Damping performance of Al + A and Al + S are similar and Al + PA is a little better than those.

3.3 Numerical Analysis

3.3.1 Simulation

From the measured results the material parameters of aluminum beam and epoxy adhesive were estimated. With respect to the material constants for the SMA foils, we assumed that they were the same as those for the wire used in the preliminary experiment etc. Moreover, it was assumed that rearrangement between R+ phase and R– phase took place in the R phase foils. The material constants of the aluminum beam, the epoxy adhesive, and the foils are listed in Table 2 (Ikeda et al. 2004), where the subscripts S, R, R+, and R– denote the quantities on the stainless steel, R phase SMA, R+ and R– phase SMA, respectively. It is assumed $T_r = T_S$.

Figure 7 shows the envelopes of the positive side of the calculated damping vibration of the beams. The simulated result seems to be in qualitatively good agreement with the experiment, although the damping of Al + PA is less than Al + S, being different from the experiment.

Table 2 Constants of the aluminum beams, the epoxy adhesive layer, the stainless steel foil, the SMA foils and the surroundings (Ikeda et al. 2004)

L mm	B mm	H_{Al} mm	H_{Ep} mm	H_R mm	H_A mm	H_S mm
200	20	2	0.08	0.04	0.05	0.04
E_{Al} GPa	E_{Ep} GPa	E_R GPa	E_A GPa	E_M GPa	E_S GPa	η_{Al}
73.0	4.64	26.7	43.3	22.9	200	0.002546
η_{Ep}	η_S	μ_{Al} kg/m	μ_{Ep} kg/m	μ_R kg/m	μ_A kg/m	μ_S kg/m
0.06136	0.003501	0.1040	0.0038	0.0090	0.0112	0.0126
ε_{pre}	ε_A	ε_M	ε_{R+}	ε_{R-}	A/V_A m^{-1}	A/V_R m^{-1}
0.02	0	0.0304	0.042	–0.042	2.0×10^4	2.5×10^4
M g	α_T K^{-1}	C MJ/(m^{3}K)	T_S K	$T_{A \leftrightarrow M}$ K	h W/(m^{2}K)	Δs MJ/(m^{3}K)
144.6	1.04×10^{-5}	2.97	291.2	248.6	43.4	–0.246
$\alpha \rightarrow \beta$	$\Psi_{c1,\alpha\rightarrow\beta}$ MJ/(m^3)	$\Psi_{c2,\alpha\rightarrow\beta}$ MJ/(m^3)	$a_{1,\alpha\rightarrow\beta}$	$b_{\alpha\rightarrow\beta}$	$a_{2,\alpha\rightarrow\beta}$	
A → M	0	2.81	10^{10}	1	10^6	
M → A	0	2.81	10^{10}	1	10^6	
R+ → R–	0	9.9	10^4	1	10^4	
R+ → R–	0	9.9	10^4	1	10^4	

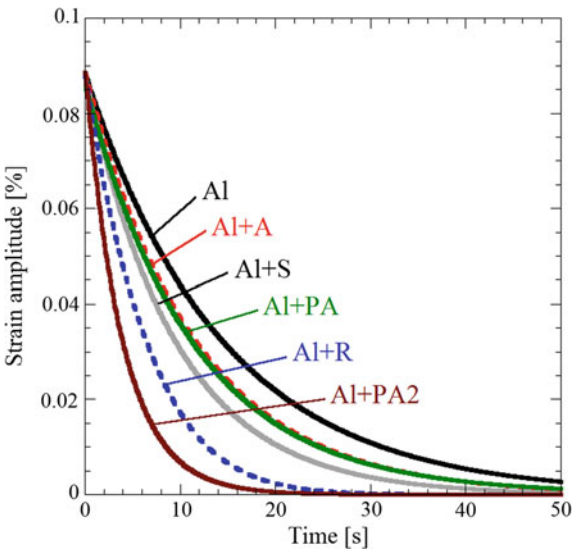

Fig. 7 Predicted envelope of damping vibration wave (Ikeda et al. 2004)

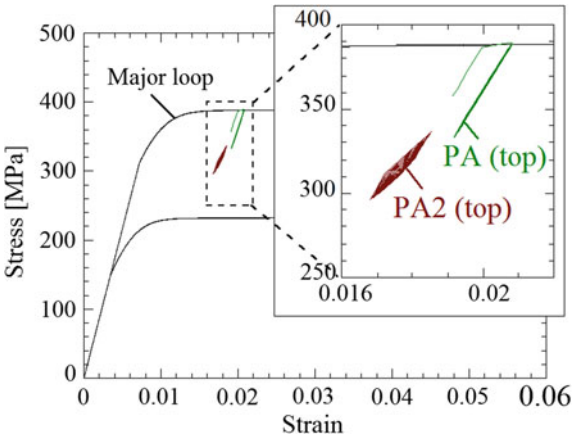

Fig. 8 Stress-strain relationship of the top SMA foil (Ikeda et al. 2004)

It can be seen from Figs. 6 and 7 that bonding R phase SMA is effective for the damping enhancement and that the modeling of the beam with a tip mass and SMA foils bonded is reasonable.

3.3.2 Effect of Prestrain of SMA Foils

The austenitic SMA foils were prestrained because we expected SMA to vibrate around the center of the major stress-strain hysteresis loop. However, we could not obtain a good damping enhancement for Al + PA beam, where the austenitic SMA foils were stretched by 2% and bonded on the aluminum beam. Since the damping performance relates to the area of the stress-strain loop, we examined the area for Al + PA beam in the simulation. The stress-strain relationship of the top SMA foil of Al + PA beam during the vibration is illustrated in Fig. 8. It was found that we could not obtain a large hysteresis loop in this condition because the deformation of SMA foil was in an elastic range and no transformation took place. Therefore, we tried simulating vibration of a beam with SMA foils which were stretched and relaxed a little before bonded so as to actually vibrate around the center of the hysteresis loop (Al + PA2). The envelope of the simulated damping vibration of Al + PA2 beam is also illustrated in Fig. 7. In this beam we could obtain a damping performance as good as Al + R beam. At this time the area of the stress-strain relationship increased as shown in Fig. 8.

4 Conclusion

A constitutive model of SMAs referred to as the one-dimensional phase transformation model, has been developed. This model can reproduce dynamic behavior of martensitic and austenitic SMAs quantitatively. The numerical example showed

that a martensitic SMA bar transforms to an austenitic SMA bar after several cyclic loadings at high strain rate, because the generated heat due to the hysteresis can not transfer to the surroundings and the temperature increases to the inverse-transformation temperature.

Next this model was applied to damping enhancement analysis. A beam model with a tip mass and bonded SMA foils was formulated. Beams with SMA foils bonded were also manufactured. The predicted and measured waves of the damping vibration were in qualitatively good agreement with each other. The results showed that bonding R phase SMA was effective for damping enhancement and bonding austenitic SMA might increase damping performance by giving proper mechanical or/and thermal treatment.

Acknowledgements The author would like to thank Mr. Yoshitaka Hata and Mr. Hidetaka Hattori for their support in experiment and calculation.

References

Barbarino S, Saavedra Flores EI, Ajaj RM, Dayyani I, Friswell MI (2014) A review on shape memory alloys with applications to morphing aircraft. Smart Mater Struct 23(6):063001 (19 pp)

Bertram A (1982) Thermo-mechanical constitutive equations for the description of shape memory effects in alloys. Nucl Eng Des 74(2):173–182

Boller C, Konstanzer P, Matsuzaki Y, Ikeda T (2001) Damping with shape memory alloys for structural systems. In: Proceedings of eleventh international conference on adaptive structures and technologies, pp 336–343

Boyd JG, Lagoudas DC (1996) A thermodynamical constitutive model for shape memory materials. Part I. The monolithic shape memory alloy. Int J Plast 12(6):805–842

Brinson LC (1993) One-dimensional constitutive behavior of shape memory alloys: thermomechanical derivation with non-constant material functions and redefined martensite internal variable. J Intell Mater Syst Struct 4(2):229–242

Falk F (1983) One-dimensional model of shape memory alloys. Arch Mech 35(1):63–84

Gall K, Sehitoglu H (1999) The role of texture in tension-compression asymmetry in polycrystalline NiTi. Int J Plast 15(1):69–92

Gandhi F, Chapuis G (2011) Passive damping augmentation of a vibrating beam using pseudoelastic shape memory alloy wires. In: Proceedings of eleventh international conference on adaptive structures and technologies, pp 319–335

Graesser EJ, Cozzarelli FA (1991) Shape-memory alloys as new materials for aseismic isolation. J Eng Mech 117(11):2590–2608

Ikeda T (2005) Modeling of ferroelastic behavior of shape memory alloys. Proc SPIE 5757:344–352

Ikeda T (2006) Application of one-dimensional phase transformation model to tensile-torsional pseudoelastic behavior of shape memory alloy tubes. Proc SPIE 6166:61660Z (8 pp)

Ikeda T (2008) Constitutive model of shape memory alloys for asymmetric quasiplastic behavior. J Intell Mater Syst Struct 19(5):533–540

Ikeda T, Nae FA, Naito H, Matsuzaki Y (2004a) Constitutive model of shape memory alloys for unidirectional loading considering inner hysteresis loops. Smart Mater Struct 13(4):916–925

Ikeda T, Hattori H, Matsuzaki Y (2004) Numerical analysis of damping enhancement of a beam with shape memory alloy foils bonded. In: Proceedings of ICAS 2004, ICAS 2004-5.2.1 (8 pp)

Ivshin Y, Pence TJ (1994) A thermomechanical model for a one variant shape memory material. J Intell Mater Syst Struct 5(4):455–473

Kamita T, Matsuzaki Y (1998) One-dimensional pseudoelastic theory of shape memory alloys. Smart Mater Struct 7(4):489–495

Leclercq S, Lexcellent C (1996) A general macroscopic description of the thermomechanical behavior of shape memory alloys. J Mech Phys Solids 44(6):953–980

Liang C, Rogers CA (1990) One-dimensional thermomechanical constitutive relations for shape memory materials. J Intell Mater Syst Struct 1(2):207–234

Machado LG, Lagoudas DC (2008) Thermomechanical constitutive modeling of SMAs, shape memory alloys—modeling and engineering applications. In: Lagoudas DC (ed) Springer Science+Business Media, LLC, New York, pp 121–187

Matsuzaki Y, Naito H, Ikeda T, Funami K (2001) Thermo-mechanical behavior associated with pseudoelastic transformation of shape memory alloys. Smart Mater Struct 10(5):884–892

Müller I (1989) On the size of the hysteresis in pseudoelasticity. Continuum Mech Thermodyn 1(2):125–142

Nae FA, Matsuzaki Y, Ikeda T (2003) Micromechanical modeling of polycrystalline shape-memory alloys including thermo-mechanical coupling. Smart Mater Struct 12(1):6–17

Ortín J (1992) Preisach modeling of hysteresis for a pseudoelastic Cu-Zn-Al single crystal. J Appl Phys 71(3):1454–1461

Otsuka K, Ren X (2005) Physical metallurgy of Ti-Ni-based shape memory alloy. Prog Mater Sci 50(5):511–678

Otsuka K, Wayman CM (eds) (1998) Shape memory materials. Cambridge University Press, Cambridge

Patoor E, Eberhardt A, Berveiller M (1995) Micromechanical modelling of the superelastic behavior. Journal de Physique IV 5-C2, C-2-501-C2-506

Raniecki B, Lexcellent CH, Tanaka K (1992) Thermodynamic models of pseudoelastic behavior of shape memory alloys. Arch Mech 44(3):261–284

Seelecke S (1996) Equilibrium thermodynamics of pseudoelasticity and quasiplasticity. Continuum Mech Thermodyn 8(5):309–322

Sun QP, Hwang KC (1993) Micromechanics modelling for the constitutive behavior of polycrystaline shape memory alloys—I. Derivation of general relations. J Mech Phys Solids 41 (1):1–17

Tanaka K (1986) A thermomechanical sketch of shape memory effect: one-dimensional tensile behavior. Res Mechanica 18(3):251–263

Thomson P, Balas GJ, Leo PH (1995) The use of shape memory alloys for passive structural damping. Smart Mater Struct 4(1):36–42

Tobushi H, Matsui R, Takeda K, Pieczyska EA (2013) Material properties of shape memory materials. Nova Science Publication, New York

Yamauchi K, Ohkata I, Tsuchiya K, Miyazaki S (eds) (2011) Shape memory and superelastic alloys: applications and technologies. Woodhead Publishing Limited, Oxford, Cambridge, Philadelphia, New Delhi

http://www.springer.com/978-3-319-53305-6

Advances in Shape Memory Materials
In Commemoration of the Retirement of Professor
Hisaaki Tobushi
Sun, Q.-P.; Matsui, R.; Takeda, K.; Pieczyska, E.A. (Eds.)
2017, X, 241 p., Hardcover
ISBN: 978-3-319-53305-6